

## Fabrication challenges for indium phosphide microsystems

This content has been downloaded from IOPscience. Please scroll down to see the full text.

2015 J. Micromech. Microeng. 25 043001

(<http://iopscience.iop.org/0960-1317/25/4/043001>)

View [the table of contents for this issue](#), or go to the [journal homepage](#) for more

### Download details:

This content was downloaded by: npsiwak

IP Address: 129.2.109.96

This content was downloaded on 27/03/2015 at 21:08

Please note that [terms and conditions apply](#).

## Topical Review

# Fabrication challenges for indium phosphide microsystems

N P Siwak<sup>1,2</sup>, X Z Fan<sup>1</sup> and R Ghodssi<sup>1</sup>

<sup>1</sup> MEMS Sensors and Actuators Lab (MSAL), A V Williams Building, Department of Electrical and Computer Engineering, Institute for Systems Research, University of Maryland, College Park, MD 20740, USA

<sup>2</sup> Laboratory for the Physical Sciences, 8050 Greenmead Drive, College Park, MD 20740, USA

E-mail: [npsiwak@gmail.com](mailto:npsiwak@gmail.com)

Received 17 September 2014, revised 9 December 2014

Accepted for publication 30 December 2014

Published 17 March 2015



## Abstract

From the inception of III–V microsystems, monolithically integrated device designs have been the motivating drive for this field, bringing together the utility of single-chip microsystems and conventional fabrication techniques. Indium phosphide (InP) has a particular advantage of having a direct bandgap within the low loss telecommunication wavelength (1550 nm) range, able to support passive waveguiding and optical amplification, detection, and generation depending on the exact alloy of In, P, As, Ga, or Al materials. Utilizing epitaxy, one can envision the growth of a substrate that contains all of the components needed to establish a single-chip optical microsystem, containing detectors, sources, waveguides, and mechanical structures. A monolithic InP MEMS system has, to our knowledge, yet to be realized due to the significant difficulties encountered when fabricating the integrated devices. In this paper we present our own research and consolidate findings from other research groups across the world to give deeper insight into the practical aspects of InP monolithic microsystem development: epitaxial growth of InP-based alloys, etching techniques, common MEMS structures realized in InP, and future applications. We pay special attention to shedding light on considerations that must be taken when designing and fabricating a monolithic InP MEMS device.

Keywords: InP MEMS, monolithic integration, III–V semiconductors, optical MEMS, microsystems

(Some figures may appear in colour only in the online journal)

## 1. Introduction

III–V materials have long been studied for use in high performance electronic and optical systems. The maturation of epitaxial growth techniques has allowed researchers to grow compound semiconductors with nearly arbitrary compositions, exhibiting widely variable mechanical and electrical properties. The ability to dictate parameters such as the bandgap, refractive index, and etching selectivity of each individual layer has broadened the scope and vision of researchers and expanded the field of compound semiconductors into previously unexplored territories.

The initial push for the use of compound semiconductors stemmed from the very high electron mobilities, mean-free-paths and the direct-bandgap electronic structure possessed by III–V semiconductors over traditional silicon based technologies [1]. Many authors have highlighted the high speed transistor technologies made possible through the development of InP–GaAs compound semiconductor epitaxy. Devices such as HEMTs [2], MODFETs [3], and integrated optical receivers/HEMTs [4] are made possible through the unique electronic properties of III–V semiconductors.

A primary advantage of III–V materials is their variable direct bandgap via the processes that enable growth

of materials exhibiting optical gain. GaAs was one of the frontrunners in this field of solid-state optics with a maximum bandgap wavelength of  $\sim 870$  nm, sufficient for early generation communication systems. With the transition to longer wavelength communications technologies, particularly 1550 nm, InP soon emerged as an alternative material system to enable the fabrication of longer-wavelength active devices (1660–925 nm) [5, 6]. The continued quest for high speed communication technologies combined with the ability to create active optical elements and high speed electronics in InP simultaneously brought about the first monolithic integration of these optical and electrical components, such as high speed optical receivers and modulators [4].

In recent years, microelectromechanical systems (MEMS) using InP-based materials have been investigated to augment these optical networks [7]. A number of examples have been reported in literature of optical modulators, demultiplexers [8–13], and couplers [14, 15] all designed in III–V materials to facilitate monolithic integration of these optical components with photodetectors and sources. To our knowledge, there have not been any examples which have demonstrated full monolithic integration of these MEMS components with their active optical elements (sources and detectors) for a variety of reasons. The goal of this review is to present relevant literature related to InP MEMS devices and to discuss the challenges that arise in developing integrated optical MEMS in these less-common materials. We have broken this paper into sections which reflect the key investigations and devices developed in InP MEMS discussing the particular impact of the research on the InP MEMS community as a whole. It is our goal to shed light on the current state of the InP MEMS field and provide an outlook for future investigations and device potential.

## 2. Materials

Indium phosphide (InP) is a compound semiconductor with a direct electronic bandgap which allows for the direct conversion of electron transitions to photons. This bandgap is tuned to correspond to energies in the near IR range by alloying InP with various materials (Ga, As, Al). In addition to these direct bandgap states and alloys, electron mobility in this semiconductor is very high, leading it to be investigated for high-speed solid-state electronics [16]. More importantly, the direct bandgap wavelength in the fiber-optic communications band (1550 nm) has brought considerable attention to this material for optoelectronic applications. Along with this came the study of using these materials for MEMS applications, particularly in the case of optical waveguiding and filtering for optoelectronic DWM communication technologies. Each of these research thrusts have benefitted greatly from the high levels of control that these alloyed material systems present to the designer, from adjusting the electrical and optical characteristics of the semiconductor crystals, to changing material properties.

This material composition is very important in III–V semiconductor systems for controlling the optical and electrical

properties, as well as the mechanical properties such as stress/strain. The ability to design layers specifically strained is beneficial when controlling valence and conduction band offsets and material bandgaps for optoelectronic devices. In the case of fabricating suspended structures for use in MEMS applications, this strain control allows for the realization of long, smooth, suspended structures. The nature of common molecular beam epitaxy (MBE) and metal organic vapor phase epitaxy (MOVPE) growth techniques enable these single-crystal alloy compositions to be grown with a very high accuracy and with nearly perfect interfaces (1–2 monolayers) between varying compositional alloys [17, 18].

With MBE, MOVPE, and other epitaxial growth techniques already established in their own respective fields, the initial studies into using InP for MEMS applications specifically focused on investigating the mechanical properties of these semiconductors. Just as was performed with silicon-based MEMS [19], these works considered basic mechanical properties and how they compare at the microscale, as these are the most important when considering microstructure design. Using beam bending and nanoindentation techniques to measure the Young's modulus, hardness, and fracture strength, Greek and Pruessner each determined that although epitaxially grown low-defect InP is weaker than silicon, it is still a sufficiently robust material for typical low-displacement MEMS applications exhibiting an average Young's modulus of about 61–106 GPa varying depending on the crystal orientation and measurement technique [20–23]. The polyatomic zincblende crystal of these materials does not exhibit the same surface symmetry in each crystal direction like the monatomic diamond structure of Si. This causes different atoms to be exposed on different planes, changing the surface properties depending on the crystal orientation. Growth conditions are also very important to the final properties of the layers, with cross contamination reported, particularly when growing arsenic-containing materials [24].

## 3. Fabrication

The field of MEMS has matured substantially since the first demonstrations of suspended structures in silicon-based materials. Transferring this microstructure formation into a different semiconductor system introduces a number of additional challenges, particularly if one is designing optical devices. In turn it also demonstrates advantages when using the aforementioned InP lattice matched materials such as piezoelectricity, tunable direct bandgaps, and highly controllable layer thicknesses. This enables a wide variety of materials with varying characteristics to be grown, even on the same substrate.

The basic processes in the surface micromachining of movable MEMS devices are the implementation of the device/sacrificial layer design scheme, and (generally) plasma-based anisotropic etching. MEMS have had a long history of being fabricated with silicon-based technology, utilizing SiO<sub>2</sub> release layers and common silicon etching techniques to fabricate various mechanical structures such as cantilevers, beams, membranes, and actuators [25]. The combination of

highly anisotropic etching processes and highly selective undercutting layers make these MEMS structures possible. The equivalent of silicon-on-insulator (SOI) materials in the lattice-matched InP system is less common, particularly when considering MEMS applications. A different method of obtaining thin, low defect, single crystal device layers with a highly selective release layer needs to be used to obtain long-term and robust solutions.

A multitude of III–V alloys lattice matched to InP substrates [22, 26] are available to be grown via various forms of epitaxy. The variety of differing alloys allows for varied materials that have etching selectivity to composition and crystal planes. The use of epitaxy allows for abrupt interfaces between selective materials, and also provides atomically smooth surfaces after undercutting; an important consideration for filters and mirror structures. Selective release layers, low loss single crystal waveguides and mirrors, low-defect semiconductor growths, and material robustness all need to be considered when designing mechanical structures in a particular material [23]. Excellent etch selectivity is common in InP lattice-matched quaternary and ternary layers, and thus the use of single-crystal release layers is ubiquitous in InP, and nearly all III–V MEMS applications [9, 10, 12, 18, 26–31]. A caveat to this is, however, since InP and lattice matched alloys are zincblende compound semiconductors, they show anisotropy based upon crystallographic orientation [18]. Depending on the sacrificial layer used, care must be taken to orient structures properly to achieve the proper undercutting profile. Devices which require high material selectivity in order to fabricate, as well as very smooth interfaces, will often rely on these wet etching techniques for release layers. Out-of-plane tunable Fabry–Perot filters, for example, require small dimensions between materials and high tolerances to achieve high finesse. This can be achieved easily by utilizing the atomic smoothness and thickness control between successive materials in a growth stack that are nearly 100% selective from each other in a wet etching solution.

As new designs which incorporate active and passive optical structures are studied and developed, this etch selectivity can become a liability in fabrication processes when attempting to integrate materials with varying bandgaps, thicknesses, doping concentrations, etc. Each of these factors change the wet etch selectivity as well as the electrical and mechanical properties. A particular concern when performing an undercutting etch in a complex III–V growth with many different layers is the selectivity of every layer exposed during the undercutting process, as this may introduce unwanted material removal.

Suspended structures formed via surface micromachining experience high probability of stiction effects which cause the released beams or membranes to adhere to surfaces of close proximity. This stiction failure can occur during the fabrication process after the undercut and subsequent drying process, or it can be induced during operation or storage. Prevention of stiction both during and post processing has been studied extensively by researchers [32]. The most common processing methods to dry released structures are CO<sub>2</sub> critical-point drying and sublimation drying. These particular methods only

prevent stiction during and immediately after the fabrication of the devices. Additional treatments which are performed to prevent stiction during device operation include applied surface passivation layers, geometry modifications and re-surfacing techniques.

Surface micromachining requires the device layer to be patterned before the undercutting process can be performed. Wet etching is the most common and the simplest method for performing this. The varying crystallographic anisotropy of wet etchants in InP lattice matched alloys mentioned above [18, 26] can make the patterning of complex geometries very difficult if not impossible. Additionally, vertical sidewalls are often required in this patterning step, which can be more difficult to control in all crystallographic directions using wet etching techniques. One must move to dry etching plasma techniques to obtain higher versatility in processing parameters, and indeed, the most recent examples of InP-based MEMS have moved towards using these methods for fabrication.

Dry etching techniques involve the use of gases and plasmas to etch materials. While some examples of InP etching using gases have been reported, the term ‘dry etching’ usually refers to plasma-based processing. The major technologies used to dry etch InP are: reactive ion etching (RIE), electron cyclotron resonance (ECR), and inductively coupled plasma (ICP). The best examples of RIE etching utilize CH<sub>4</sub>/H<sub>2</sub> chemistries, but polymer buildup, hydrogen passivation of dopants, and a slow etch rate ( $\sim 100 \text{ nm min}^{-1}$ ) make this technology less attractive [33–37]. Some solutions using this RIE etch chemistry use a cyclic etching method that mimics the Bosch process with a CH<sub>4</sub>/H<sub>2</sub> etch cycle and a O<sub>2</sub> plasma etch step to remove excess passivation. The final result is a very vertical and scalloped sidewall [15, 38, 39]. One of the best etchants for InP materials is Cl<sub>2</sub>, however the InCl<sub>x</sub> byproducts of this etch will not desorb from the surface unless samples are elevated in temperature above 175 °C [40]. The accumulation of these byproducts can create micromasking and rough and sloped sidewalls. Even at elevated sample temperatures, the traditional RIE etch environment cannot achieve vertical sidewalls with Cl<sub>2</sub> plasma chemistry [41].

ECR and then ICP etching were later introduced to achieve higher etch rates and more vertical and smooth sidewalls particularly using Cl<sub>2</sub> plasmas. Both of these technologies provide much higher ion densities than traditional RIE etching and provide better control over the ion energy. Pure Cl<sub>2</sub> plasma etching in ICP at elevated temperatures has very high etch rates ( $\sim 2 \mu\text{m min}^{-1}$ ) but exhibit undercut profiles and damaged etch surfaces [33–35, 42]. This is due to the nearly pure chemical nature of the Cl etching mechanism and its isotropic etch behavior. In order to provide vertical and smooth etching conditions, one must introduce *in-situ* passivation to the sidewalls or increased ionic bombardment to increase the surface energy in the direction of the etch to promote anisotropic etch rates. One way to achieve this is by adding other gases to the chamber during etches such as H<sub>2</sub>, Ar, He, N<sub>2</sub>, O<sub>2</sub>, CH<sub>4</sub> to increase the etch uniformity and the anisotropy of the etch [35, 42–44]. H<sub>2</sub> and CH<sub>4</sub> particularly help to balance the chemical reactions between the III and the V components of the

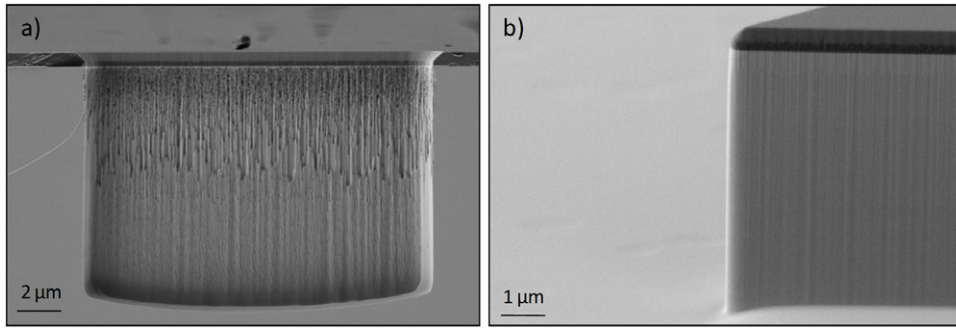


**Figure 1.** SEM images showing the effects of mask erosion (a) and reduced mask erosion after process development (b).

compound semiconductors and to thus promote even removal of material, decreasing roughness. Ar and He provide a physical component to the etching process, increasing the surface energy of the horizontal interfaces during the etch.  $N_2$ ,  $O_2$ , and  $CH_4$  provide passivation in the form of oxides, nitrides, and polymers that form on the vertical sidewalls during the etching, further increasing etch anisotropy and increasing sidewall quality. Excess generation of these polymers and passivation layers can impede further processing steps if not removed or able to be removed from the sample surface after the etching. Due to the low volatility of the Cl byproducts other chemistries have been investigated utilizing HBr as the reactive gas which does not have this elevated temperature requirement. Similar etch rates, etching mechanisms, and final resulting profiles have been found utilizing this chemistry instead of the more traditional Cl-based chemistry [42, 43, 45–52].

ECR and ICP etching can have stringent requirements on the etch masking material used [53]. In nearly all cases of InP plasma etching, the masking material is critical to the final sidewall profile, both related to verticality and sidewall roughness. Angle of the mask sidewall and mask edge roughness all directly transfer into the underlying substrate during etching. Furthermore, erosion of the masking material can result in sidewall damage and sloping as is evident in figure 1. Photoresist can be used as a hardmask in limited cases (RIE) if hardened properly. The high powers and temperatures involved in etching with ECR or ICP, however, render this method impractical or impossible due to high removal rate of the mask. This necessitates using more robust methods for masking the etch such as dielectrics ( $SiO_2$ ,  $Si_3N_4$ ), metals (Al, Ni, Ti), or a combination of these materials.  $SiO_2$  and Ni are often favored as mask materials due to their robustness during the etching process, and somewhat more importantly, their ease of removal following the etch. Using another material instead of photoresist as an etching mask will introduce an additional step in the fabrication process (mask fabrication) which needs to be finely tuned to prevent erosion, maintain sidewall smoothness, and ensure a clean pattern transfer into the eventual semiconductor material.

Possibly more important is the control of the chamber condition, which has been shown to greatly affect etching characteristics [33, 38] depending widely on the etch chemistry used. This is particularly true for polymer-generating chemistries such as  $CH_4$ -based etching which tend to leave polymer and byproduct depositions on the chamber walls. It is

also something of consideration when working in a multi-user facility where the chamber is exposed to many different etch processes or materials that leave different or unknown byproducts. It is important then to establish a routine for cleaning and conditioning (coating the chamber walls) so that each etch run is performed with comparable conditions [33, 38]. In many cases even the sample carriers (predominantly Si,  $Al_2O_3$ , and  $SiO_2$ ) required to process single die with full-wafer processing equipment contribute to the composition of the sidewall passivation and can strongly affect the quality of the finished etch, and thus must be considered when developing a final etching process [42].

While these different etching techniques have clearly been studied extensively, they have often focused on more traditional microelectronic or optoelectronic technology development, and not on InP MEMS devices specifically which are very diverse in their material choices and physical design requirements (dimensions or complexity). In-depth understanding of every fabrication processing step coupled to the device and process design is absolutely required when performing high-complexity monolithic InP MEMS systems; failure to do so will not only reduce final device performance, it can often result in total device failure. Table 1 shows a summary of the most common etching techniques used for InP MEMS devices and references which describe these different etching techniques in more detail.

#### 4. Optomechanical filters

Optomechanical filters were a popular research topic in the 1990s and 2000s, primarily targeting applications in fiber communications and spectroscopic sensing. Fabry–Perot resonators are often used for interferometry, and also for narrow band optical filtering in applications such as data communication (e.g. DWDM) and sensors (e.g. spectroscopy). A wide and continuous tuning is often desirable for such applications to broaden their respective capabilities.

Tunable-wavelength lasers and wavelength division multiplexing are both required to increase the transmission bandwidth and the routing capability of optical communications. Tunable semiconductor lasers have been traditionally achieved through monolithic integration of edge emitting devices with a tunable filter to tune the laser wavelength and a phase-shifting component to select a particular longitudinal mode. These filters

**Table 1.** Table of InP etching techniques. Note that values such as mask selectivity and etch rate are often not provided in publications, and thus some generalities have been made for the sake of comparison.

InP etching techniques						
Etch method	Typical chemistries	Masking material	Etch rates	Mask selectivity	Comments	References
Wet chemistry	FeCl <sub>3</sub> :H <sub>2</sub> O	Photoresist, SiO <sub>2</sub> , Si <sub>3</sub> N <sub>4</sub>	0.1–1 μm min <sup>-1</sup>	Very high in most cases; nearly infinite	Mostly used for undercutting and device release due to etch isotropy. Chemistry should be chosen to not interfere with other materials on the device wafer.	[9, 10, 12, 18, 26–31]
	HF:H <sub>2</sub> O <sub>2</sub> :H <sub>2</sub> O				Selectivity of undercut layers will vary based upon material composition and etchants used (see [26] for details).	
	H <sub>2</sub> SO <sub>4</sub> :H <sub>2</sub> O <sub>2</sub> :H <sub>2</sub> O H <sub>3</sub> PO <sub>4</sub> :H <sub>2</sub> O <sub>2</sub> :H <sub>2</sub> O C <sub>6</sub> H <sub>8</sub> O <sub>7</sub> :H <sub>2</sub> O <sub>2</sub> :H <sub>2</sub> O					
RIE (Plasma)	CH <sub>4</sub> /H <sub>2</sub> , CH <sub>4</sub> /H <sub>2</sub> + O <sub>2</sub> , CH <sub>4</sub> /H <sub>2</sub> /Ar + O <sub>2</sub>	Photoresist, SiO <sub>2</sub> , Si <sub>3</sub> N <sub>4</sub> , NiCr, Ti	0.3–1 μm min <sup>-1</sup> (cyclic)	>50:1. Selectivity can vary depending on gas mixtures. Hard-masks (oxides, nitrides, metals) fare better than photoresists due to long etch times and oxygen in the etch cycles.	Deep etching requires cyclic etching of CH <sub>4</sub> /H <sub>2</sub> and O <sub>2</sub> due to the low volatility of byproducts and high polymer buildup. Does not require special plasma etching chambers or elevated sample temperatures.	[33, 36–39, 41, 54]
	CH <sub>2</sub> /Ar/H <sub>2</sub> , BCl <sub>3</sub> /Cl <sub>2</sub> /H <sub>2</sub> , Cl <sub>2</sub> /(He, N <sub>2</sub> ) HBr/H <sub>2</sub>	SiO <sub>2</sub> , Si <sub>3</sub> N <sub>4</sub> , NiCr, Ti	0.1–4.8 μm min <sup>-1</sup>	>10:1. Mostly dependent on the physical bombardment of the mask, not chemical etching damage.	Plasma etching variants consist of a halogen species and other additives to improve anisotropy. InP etching requires elevated sample temperatures > 100 °C due to involatile InCl <sub>x</sub> byproducts. Strong dependence can be observed on the cover-plate material used during etching (Si, Al, Al <sub>2</sub> O <sub>3</sub> , SiO <sub>2</sub> )	[33–35, 40, 42–44, 46, 47, 53, 55–59]

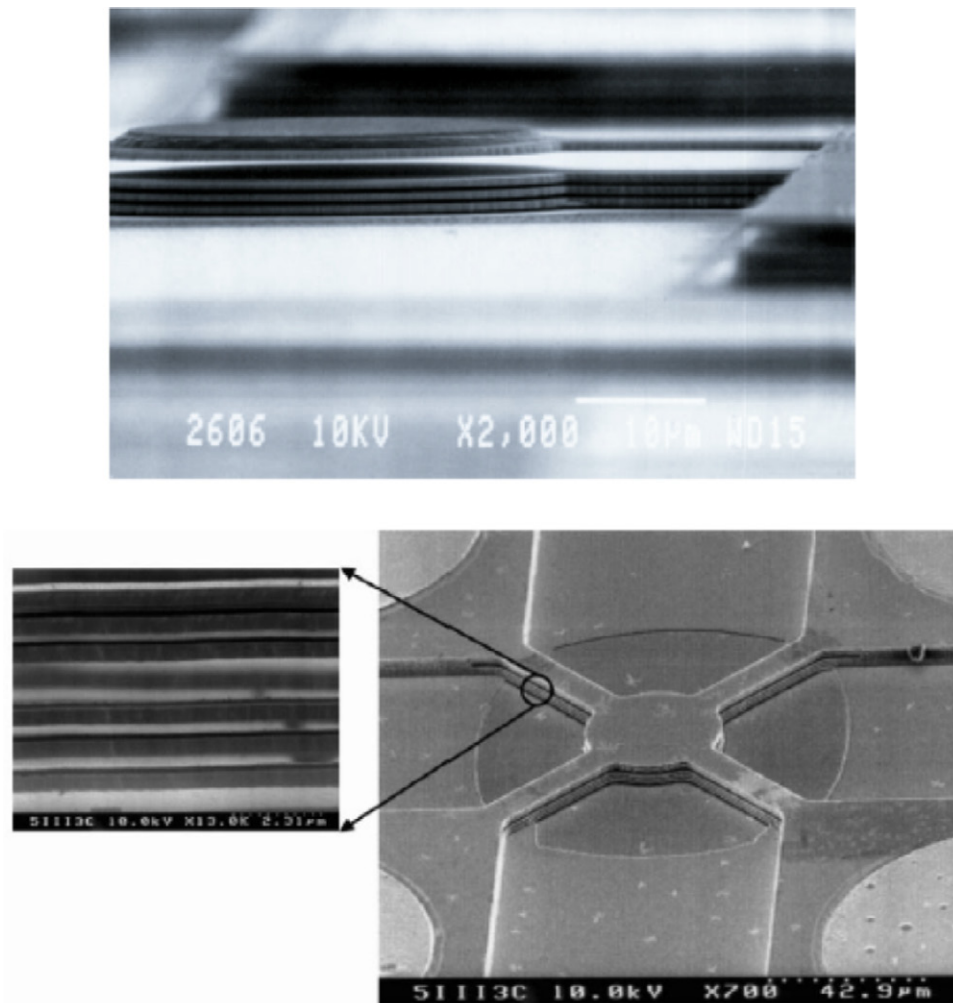


**Figure 2.** Examples of out-of-plane tunable-cavity Fabry–Perot filters demonstrated in InP. Top image reprinted from [64]. Copyright 2000, with permission from Elsevier. Bottom image reprinted with permission from [65]. © 2003 IEEE.

are usually tuned by modulating the refractive index which has limited continuous tuning range, typically within 1% (<10 nm). Other desirable traits include low-powered, high-speed, high extinction ratio, no polarization dependence, and simple coupling. These traits listed can all be satisfied with the development of microfabricated tunable Fabry–Perot platform for a tunable filter, source, and photodetector.

Tunable vertical cavity Fabry–Perot resonators are typically made of transparent plates with two moveable parallel reflecting mirrors, creating an optical cavity. The resonant condition is exhibited as high peaks in the transmission spectrum of the filter. By tuning the cavity condition of the resonator, the transmitted wavelength can be shifted. Micro-tunable Fabry–Perot filters are typically fabricated using thin alternating layers of dielectric and air to form Bragg gratings, examples of which can be seen in figure 2. By changing the spacing between the mirrors, resonant wavelengths can be changed. The first demonstration of a vertical coupled-cavity tunable filter was shown in 1995 using silicon by Tran *et al* [60] and in III–V materials by Larson *et al* [61]. Larson *et al*, in the following year, demonstrated a wide and continuous wavelength tuning in a vertical-cavity surface-emitting laser (VCSEL) by monolithically integrating a deformable top dielectric

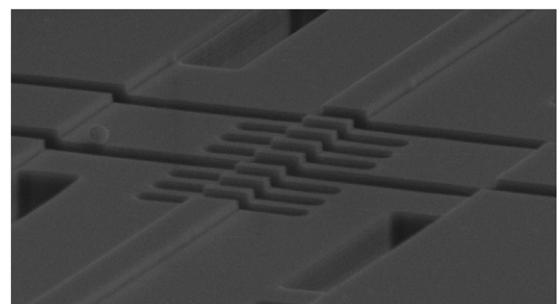


**Figure 3.** SEM image showing in-plane tunable Fabry–Perot filter using a ridge waveguide. Figure reproduced from [69].

membrane mirror above the VCSEL. Le Dantec *et al* used a bridge membrane suspension platform to demonstrate 60 nm tuning range by applying 16 V by electrostatically actuating an InGaAs Bragg mirror. Spisser *et al* used InP/air interface resulting in similar results of 62 nm tuning range using 14 V [62]. Daleidan *et al* were able to improve on its performance but showing tunability over 100 nm with an actuation voltage of only 5 V [9, 10]. Tunability was further improved by optimizing filter design via simulation and modeling to 200 nm with a 10 nm resolution [8, 63].

Deviations from conventional membrane tuning designs include torsional designs with a counterweight-cantilever type shape allows for a leveraging effect when actuated from the short side of the teeter-totter. The longer side possesses the DBRs, forming the cavity between the DBR and the substrate. 7 dB of insertion loss was observed when tested with a data link [11].

Furthermore, there have been in-plane designs which attempt to utilize etched mirrors and resonant cavities directly coupled to waveguides to more readily integrate with monolithic optical systems [66–68]. These authors utilize in-plane waveguides and a moveable beam to move one of the Bragg mirrors in-plane via electrostatic actuation. A tunable range of 12 nm was demonstrated [68]. Further work on this in-plane tunable filter utilized ridge waveguides and was able demonstrate 35 nm of tunability with 25 V of applied voltage to the electrostatic actuators shown in figure 3 [69].

Due to the stringent requirements of tunable filters for applications in optical communication, it is necessary to take into account the mechanical and optical design parameters of the Fabry–Perot cavities. Global optimization includes reduced actuation voltages, large pull-in voltage, improved device reliability, and fast switching times. Simulations and analytical modeling have been used for the purpose of satisfying these conditions, narrowing down the design parameters of the mirrors, actuation scheme, and mirror suspensions. These simulation results are used to verify experimental results. The limitations of in-plane tunable filters lie in the ability to define low-order Bragg gratings due to the constraints of lithography techniques and the lack of repeatability for dry etching procedures. Poor sidewall quality (verticality and smoothness) greatly reduces the reflectivity of the Bragg mirrors such as seen in figure 3. This is the primary reason Bragg gratings defined by dielectric or epitaxial growth have much higher finesse comparatively: it is much easier to control repeatable thicknesses and very smooth and parallel interfaces via CVD or epitaxy.

There have been some examples of tunable filters that have been integrated with photodetectors and photo emitters. Zhou *et al* described the fabrication and testing of an optically pumped, wavelength selective, and tunable light emitting diode consisting of an active region of InAs quantum dots and a MOEM tunable filter made of InP/air gap layers. They demonstrated an enhancement of the spontaneous emission by a factor of about 40 at the resonant wavelength of 1500 nm. This device exhibited a tuning range of more than 50 nm using a voltage of up to 15 V [70]. Further work has developed devices which have up to 60 nm of tunable single-mode range used for gas detection and much higher output powers than the first demonstrations of these devices [71, 72]. They utilize GaAs lattice-matched epitaxial Bragg gratings which are transferred to the InP-based active region via bulk micromachining [73]. Other authors have extended the range of wavelengths using varied active regions and cavity designs, emitting single-mode light up to 1.95  $\mu\text{m}$  with InP-based materials and novel dielectric and metal-based surface micromachining techniques which increase the overall yield of devices and reduce the required operating voltages for electrostatic actuation of the tuning mirrors [74, 75]. More recently work which demonstrates very long tuning ranges of

up to 100 nm while maintaining single-mode operation has been achieved [75, 76].

Due to residual stresses caused by trace contamination in the layer growth, stress issues relating to tunable filters were reported by Tay *et al*. They analyzed the stresses of the suspensions and the mirrors using Raman spectroscopy and the deflection using white light interferometry. By varying membrane and suspension dimensions, a range of internal mirror stresses from 0.24 to 0.08 GPa were measured, highlighting the importance of suspension and device design. Based on these studies, they designed four different optimized suspension designs for a suspended Fabry–Perot interferometer filter [13, 77].

It is noted that nearly all Fabry–Perot resonant cavity structures are out-of-plane, making their future integration into monolithic InP systems very difficult if not impossible. For all of these devices, hybrid fabrication or packaging schemes are needed to interface them with lasers or external optics, introducing additional complexity in design, fabrication, and packaging. In many of these cases however the quality of the filter provided by the smooth and precise interfaces of epitaxial growth are much more important than the integration potential. More work in the fabrication of in-plane filters, or different hybrid bonding technologies can close this gap between practicality and fabrication difficulty and provide for additional avenues of integration with emerging technologies such as III–V on silicon photonic integrated circuits.

## 5. Suspended waveguide technology

A primary building block of microfabricated InP optical systems is waveguides. While many examples of InP dielectric waveguides utilize ridges in a bulk material, these designs often have low confinement and can experience substrate losses. For many applications, a tightly confined mode is desirable, and can be achieved by designing air-cladded waveguides. MEMS structures require moveable components which can only be achieved by releasing the entire structure from the device substrate. Many applications of in-plane dielectric waveguides have been realized, including in-plane resonators, filters, splitters, and sensors [78–84].

The InP material system readily enables ternary and quaternary layers to be used as sacrificial layers for suspending waveguides. Wet chemistries easily etch the sacrificial layer and undercut device layers to release waveguides from the bulk. In nearly all cases, a critical point drying method is used to prevent stiction of the devices to the substrate. This enables the refractive index of cladding on all four sides to be reduced to that of air or vacuum by subtracting the material away from underneath the waveguide. It also provides access to a building block structure for moveable MEMS.

The suspended waveguides are secured to the substrate via lateral tethers that are attached to anchoring platforms. Examples of this technology include waveguides fabricated from bulk InP alloys [67] and also examples of devices that have multiple quantum well core layers [85] to provide for nonlinear optical effects. Kelly *et al* investigated suspended

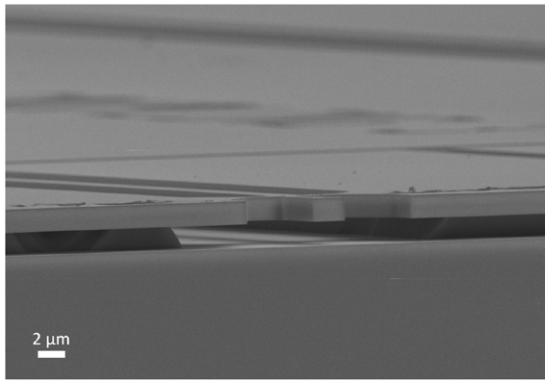


Figure 4. SEM of released and suspended waveguide facet.

InP waveguides created in quaternary waveguide layers with an  $\text{In}_{0.53}\text{Ga}_{0.47}\text{As}$  sacrificial layer. The samples are grown with MBE as  $\text{In}_{0.95}\text{Ga}_{0.05}\text{As}_{0.08}\text{P}_{0.92}$  to be slightly tensile strained, preventing buckling of long spans of suspended waveguides. The authors investigated how the propagation loss depended on the tether geometry (tether sizes) and number of tethers. They found that minimum loss for their waveguides was  $2.2\text{ dB cm}^{-1}$  with a maximum suspended length of 2.5 mm. Minimum tether loss was estimated to be  $0.09\text{ dB/tether}$ , typical loss is measured as  $0.25\text{ dB cm}^{-1}$ . Another design for suspended waveguides has been demonstrated by Ng *et al* which utilizes an  $8\mu\text{m}$  ‘S’ bend flare at the tether point intended to more tightly confine optical power in the vicinity of the tethers, reducing the scattering losses at these points and allowing for wider, more robust tether designs [86]. The authors estimate the loss of this tether design to be  $\approx 0.2\text{ dB cm}^{-1}$  [86].

Stievater *et al* additionally developed suspended waveguides with quantum well cores (20 wells) to serve as high-index-contrast devices for electro-optical applications. Using an  $\text{In}_{0.52}\text{Al}_{0.48}\text{As}$  sacrificial layer, it was demonstrated that suspended MQW waveguides can exhibit a propagation loss that is approximately  $4\text{ dB cm}^{-1}$  at wavelengths only 125–150 nm below bandgap [85]. In addition, tether losses can be as low as 0.15 dB per tether pair. Scattering was found to be more pronounced in TM modes, as the mode directly couples with the etched sidewalls while the TE modes couple to the atomically smooth epitaxial layers and thus have lower loss. These examples of InP-based suspended waveguide structures are essential components of many optomechanical structures, such as optical switches and resonator sensors. Initial examples such as shown in figure 4 require cleaving of waveguide facets to provide for low loss facet coupling.

## 6. Optomechanical switching

With the increasing complexity of optical networks, polarization and wavelength insensitive optical switches are of increasing importance. As its bandgap wavelength is below 1550 nm, this material has been of prime importance for operation at these telecommunications wavelengths. The development of surface micromachining for these material systems has enabled the realization of in-plane architectures carrying a

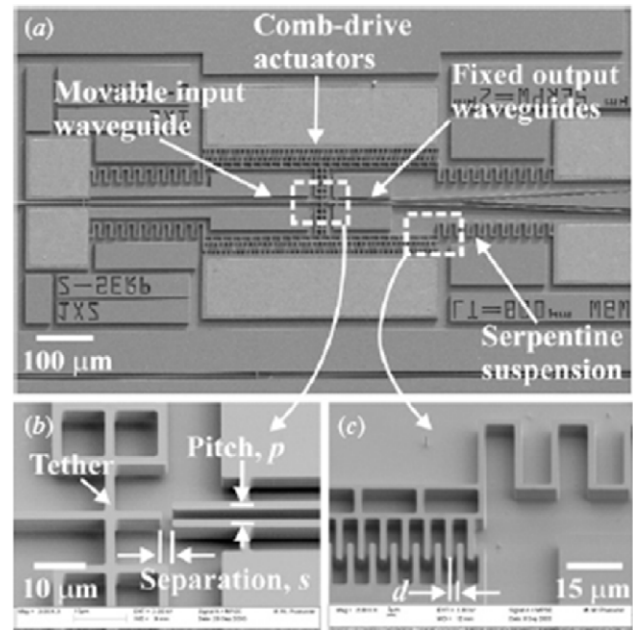


Figure 5. InP-based suspended optomechanical switch [15].

large number of optical channels. With the enabling addition of tethered waveguides in the 1990s, optomechanical switches were developed in the InP material. These optomechanical switches, in addition to supplementing routing capabilities of complex optical networks, are easily integratable with in plane waveguides and exhibit robustness, low power consumption, and low optical loss.

One of the first demonstrations of optomechanical switching was conducted by Ollier *et al* in 1995, where a  $1 \times 2$  switch was conceived using a ribbed waveguide cantilever made up of a sandwich of 3 PECVD silica layers with different phosphorus doping levels which were isotropically undercut to release the electrostatically actuated cantilever waveguide. The propagating wave inside the cantilever waveguide was butt-coupled to two static output waveguides as the cantilever was laterally aligned to each output waveguide facet as potential was applied to lateral electrodes in parallel to the cantilever beam [87]. Since then, there have been multiple groups that have iterated on this design and developed similar optomechanical switches in other materials, including a wide range of silicon based, polymer based, and finally InP-based semiconductors [14, 88–96].

The first demonstrations of tethered optomechanical switches in III–V semiconductors were fabricated in GaAs–AlGaAs and exhibited  $1 \times 2$  switching capabilities [97, 98]. Pruessner *et al* demonstrated the first InP-based  $1 \times 2$  end coupled waveguides (shown in figure 5) which demonstrated a waveguide loss of  $2.2\text{ dB cm}^{-1}$  with a coupling loss of 3.2 dB. Channel isolation was measured to be  $-26\text{ dB}$ , close to the calculated  $-30\text{ dB}$ . Switching times were measured to be  $140\mu\text{s}$  with a settling time of 2 ms for a waveguide cantilever of  $1200\mu\text{m}$  in length. The authors claim the performance of the switch is suitable for network restoration and routing applications due to the slower speeds and the increased settling time of the resonant beam structure [15].

Pruessner *et al* in 2005 demonstrated optical switching using suspended MEMS waveguide beams placed parallel to each other and actuated together electrostatically to induce evanescent coupling from one waveguide to the next using a potential of less than 10V. Channel isolation of  $-47$  dB was obtained with switching losses of 0.5 dB. Switching time for the coupler was as low as  $4\mu\text{s}$  due to the lack of a resonant settling time. A voltage-controlled variable optical coupling over a 17.4 dB dynamic range was also demonstrated [93]. More recently, Podoliak *et al* demonstrated a similar coupling scheme for an all-optical buffer using parallel suspended waveguides with varied tether geometries meant to introduce tunable propagation delay [99]. Using this coupling scheme, 100% time delay with driving voltages of 3V are predicted for final devices [99].

These devices introduce additional functionality into future photonic monolithic integration schemes including moveable air-clad waveguides and switching components. These devices which exhibit resonant behavior can be exploited for other diverse applications.

## 7. Cantilever waveguide sensors

The resonant frequency of the end coupled waveguide cantilever switches can easily be measured via the variable optical coupling experienced at the switch output during switch operation. The coupling sensitivity of the misalignment between the two waveguides is very high due to the highly confined optical modes and exhibits atomic force microscopy (AFM) level displacement resolution [100]. Highly sensitive cantilever displacement measured optically traditionally utilizes off chip bulky equipment [101–106], while these in-plane devices have much simpler instrumentation architectures. This can be seen as an advantage to using these in-plane waveguide devices as mechanical resonators; thus, a natural progression is to use these devices for cantilever-based sensing applications. There are many examples of cantilever waveguide sensors for applications in vibrational, acoustic, biological, and chemical sensing using more traditional materials such as oxynitride, silicon, and polymers [83, 100, 107–110]. However, due to the limitation of these materials, these systems all require off-chip optical sources, or at best a hybrid integration scheme if one desires to miniaturize. The integration possibility that is inherent in the InP material system due to the material growth flexibility makes these devices very attractive, allowing for the development of self-contained, optically measured, mechanical resonator systems.

Siwak *et al* utilized a cantilever waveguide in the InP material system in order to pursue true single chip sensors, capable of monolithically integrating on-chip sources and detectors with the cantilever sensor. The platform operation resembles that of Pruessner's [15, 93] and other optomechanical waveguide based switches, where a rectangular waveguide was singly clamped and functioned as a cantilever resonator. The simplified resonator design can be seen in figure 6. The cantilever waveguide was shortened to increase the resonant frequency and quality factor, enhancing the device sensitivity. InP cantilevers from 10 to  $100\mu\text{m}$  long were released using

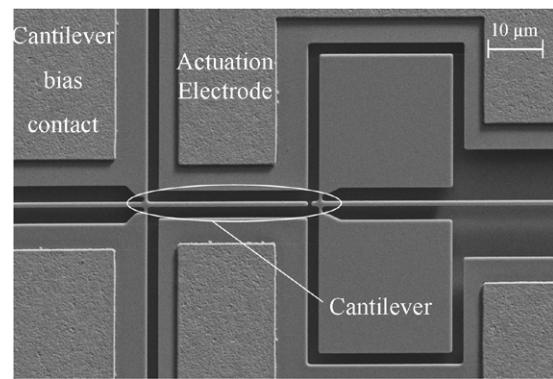


**Figure 6.** Top-down image of InP cantilever waveguide resonator [111].

the same  $\text{In}_{0.53}\text{Ga}_{0.47}\text{As}$  sacrificial layer. Electrostatic actuation of up to 26V was used for the dynamic operation. Resonant frequency ranged from 5.78 MHz to 81.1 kHz, with quality factors ranging from 300 to 10. A frequency shift due to a mass absorption of 65 Hz was measured, corresponding to a measurement of  $6.92 \pm 1.1 \times 10^{-14}$  g with a minimum detectable mass of  $5.09 \times 10^{-15}$  g for the devices reported [111].

An integrated on-chip photodetector was fabricated with these same sensor elements to eliminate the need for an off-chip detector and noise and optical loss of waveguide to off-chip fiber coupling. Using the integrated photodetector the resonant frequency of this device was measured with 60 Hz less frequency variation over a 20 min sample than previously demonstrated in systems without integrated photodiodes, with a detection limit of  $\Delta m$  of  $16.7 \times 10^{-15}$  g [112]. This is a further indication of improved device performance due to the monolithic integration of various components of the sensor system.

## 8. Discussion

The promise of MEMS devices constructed from InP semiconductors has been lauded for the last three decades, with the ultimate goal being massive parallelism and monolithic integration. While a number of these goals have been met, there have been very few examples of monolithic integration in the MEMS community. The small number of examples is illustrative of the difficulty and complexity involved in the fabrication and design process of optomechanical and optoelectronic devices [113].

Material growth itself is a major hurdle to the realization of InP microsystems. Complex monolithic MOEMS systems require significant design of material layers taking into account electrical properties of the layers, optical properties, mechanical properties, and etch selectivity. Beyond this, availability of material growths is limited, and outsourcing to foundries can often be cost prohibitive. It has been observed by our group that when attempting to generate new technology in this research area, partnerships between epitaxial semiconductor manufacturing sources and research groups are highly beneficial to the success of a design process since they allow for direct feedback between the growers, fabricators, and experimentalists.

This direct feedback is critical to solve practical issues such as doping concentration variations, film stresses, and fabrication compatibility. These are particularly important in very complex layer structure designs which incorporate a number of varying alloys of III–V materials.

In any compound semiconductor material system, interplay between various material, optical, and electrical properties are more complex and interdependent. In the InP ternary and quaternary system, you have a very wide variety of material compositions available for growth between the elements of In, Ga, As, P, Al. A particular concern when performing an etch in a complex III–V growth with many different layers is the selectivity of every layer exposed during the process. Because of this, development of any wet or dry etching processes, processes, chemical strips, liftoff processes, etc must be considered in light of every exposed epitaxial layer to prevent unwanted material erosion. Dry etching conditions will be variable as the etch proceeds through the various epilayers due to the different material composition; this makes it more difficult to establish accurate etching depth. Many systems use spectrographic endpoint detection to assist in timing etches to reach the proper depths. As a result, even with a very capable processing tool, the process needs to be finely characterized for individual processes and devices.

Alternatively when fabricating on a large stack of materials a passivation method such as a polymer coating or PECVD dielectric such as silicon nitride or silicon dioxide deposition between steps may need to be performed to protect portions of the epitaxial growth. Conformality and quality of these films are paramount. Devices may also require planarization to achieve high-resolution patterning of photoresists for future steps. A key to protecting these layers for a MEMS device often requires patternability to selectively remove the passivation from the moveable parts of the MEMS structure. As this is the case, often the method cannot be a fully encapsulating process as is seen in the microelectronics industry. Many optoelectronic devices already use benzocyclobutene (BCB) as a planarization, encapsulation, and passivation material [114–117]. It is attractive due to its robustness, processing ease, and photopatternable formulations. Other very common methods include pyrolyzed photoresist films, which offer ease of patterning, but somewhat unstable electrical characteristics due to the high carbon-containing compounds [118, 119].

Compatibility of related materials is less common in traditional MEMS material systems such as silicon and silicon dioxide, but is critical in optical MEMS development as many of the compositions that can be used a sacrificial layers are also necessary for active optical regions. Additionally most etch selective composition families are binary in nature, and thus flexibility of wet etching chemistries are limited to adjusting partial selectivities or growth layers [26, 28]. An example of this is the InP device layer— $\text{In}_{0.53}\text{Ga}_{0.47}\text{As}$  sacrificial layer material architecture. In this case the  $\text{In}_{0.53}\text{Ga}_{0.47}\text{As}$  sacrificial layer can be used as a etch susceptible layer to release InP membranes and devices, and also can be used as an optical absorber for a photodetector as was demonstrated recently in [120]. When fabricating a

system that incorporates both of these, care must be taken to protect areas from being undercut when not intended. Changing geometry or depositing protective dielectrics are common techniques used to realize this; [121] however, one can use the material alloying to obtain different absorber layer compositions which have a higher etch selectivity to the sacrificial etchant. This is often not 100% selective so some parasitic damage is to be expected [26].

Contrasting optical properties of every layer in an epitaxial wafer also need to be considered in the design of a monolithically integrated system. As with any engineering problem, many tradeoffs need to be weighed. Doping levels need to be kept low enough to prevent free carrier absorption in optically transparent regions; however they also need to be high enough to provide for good ohmic contacts to electrically probe the device in question. Regions of optical power generation, passive optical waveguiding, and optical absorption need to be present throughout the layer structure in many situations, particularly for vertically integrated schemes. These areas commonly need to operate independently from one another requiring an isolation scheme; either trench etching, material removal, or innovative annealing processes [122], each with their own drawbacks and advantages. Additionally, varying bandgaps produce layers with different absorption coefficients, requiring one to very carefully engineer the mode propagation through the whole structure rather than designing individual components and assembling them as separate entities; their properties become interdependent once such a high level of complexity is reached.

Oftentimes, researchers are forced to design sub-optimal systems if they are to be monolithically integrated together. As with highly demanding applications such as optoelectronics, these shortcomings and tradeoffs can reduce the practicality of such demonstrations. In these cases the difficulty of commercialization and large-scale fabrication of monolithic III–V MEMS elements far outweighs the potential benefit and utility that may be provided from monolithic integration. We believe, however, that this is where MEMS technology will emerge as a key technological focus due to the very broad range of applications which often do not inherently carry the same stringent optical tolerances or requirements. A prime example is the MEMS waveguide cantilever resonators presented above which utilize on-chip optical sources and detectors as low-requirement readout methods [15, 111, 112].

The field of InP MEMS has slowed down considerably due to many of these challenges; however, the field of integrated optoelectronics has not. This is promising in that new fabrication technologies, device architectures, and integration techniques are being invented and commercialized. An example is silicon–InP bonding, which can possibly be used in the future to more tightly integrate electronics with the optoelectronic components in these systems. In systems such as these, the active III–V material is fabricated separately from Si-based passive components. The advancement of bonding technologies in the recent decade has allowed for bonded active materials with more traditional CMOS fabrication that would not have been previously possible [123–127]. Each of these examples utilizes slightly

different techniques to achieve the ultimate goal of bridging the compatibility gap between Si-based CMOS and III–V fabrication. While these examples are not MEMS related InP materials specifically, they demonstrate that such integration is indeed feasible and will serve as a starting point for integration of MEMS components with integrated photonic devices. This is just one example of groups tackling some of the practical fabrication issues that arise from working with III–V materials such as dry etching, material compatibilities, and the other myriad of issues discussed above. Potential for the integration of III–V and Si materials in this fashion have recently seen much attention and investment from industry, which will drive this technology forward into mainstream microelectronics. We envision the continued development of these optoelectronic devices and their commercialization will spur on new generations of researchers who, analogous to previous generations, take these systems and find new ways to utilize the technology and apply it to existing and new areas of research.

## References

- [1] Eastman L F 1983 Use of molecular beam epitaxy in research and development of selected high speed compound semiconductor devices *J. Vac. Sci. Technol. B: Microelectron. Nanometer Struct.* **1** 131
- [2] Zurich E T H 2010 High electron mobility transistors (HEMT) [Web Page] Available ([www.mwe.ee.ethz.ch/en/about-mwe-group/research/vision-and-aim/high-electron-mobility-transistors-hemt.html](http://www.mwe.ee.ethz.ch/en/about-mwe-group/research/vision-and-aim/high-electron-mobility-transistors-hemt.html))
- [3] Peng C, Aksun M, Ketterson A, Morkoc H and Gleason K 1987 Microwave performance of InAlAs/InGaAs/InP MODFETs *IEEE Electron Device Lett.* **8** 24–6
- [4] Broekaert T P E, Jensen J F, Yap D, Persechini D L, Bourgholtzer S, Fields C H, Brown-Boegeman Y K and Walden R H 2001 InP-HBT optoelectronic integrated circuits for photonic analog-to-digital conversion *IEEE J. Solid-State Circuits* **36** 1335–42
- [5] Kasaya K, Mitomi O, Naganuma M, Kondo Y and Noguchi Y 1993 A simple laterally tapered waveguide for low-loss coupling to single-mode fibers *IEEE Photon. Technol. Lett.* **5** 345–7
- [6] Thijs P J A, Tiemeijer L F, Kuindersma P I, Binsma J J M and Van Dongen T 1991 High-performance 1.5  $\mu\text{m}$  wavelength InGaAs–InGaAsP strained quantum well lasers and amplifiers *IEEE J. Quantum Electron.* **27** 1426–39
- [7] Leclercq J L, Seassal C and Viktorovitch P 1999 InP-based micro-opto-electro-mechanical systems (MOEMS) *J. Phys. IV* **9** Pr2–123
- [8] Bondavalli P, Benyattou T, Garrigues M, Leclercq J L, Jourba S, Pautet C and Hugon X 2001 Opto-mechanical design of tuneable InP-based Fabry–Pérot filter for gas analysis *Sensors Actuators A* **94** 136–41
- [9] Daleiden J, Chitica N and Strassner M 2002 Tuneable InP-based microcavity devices for optical communication systems *Sensors Mater.* **14** 35–45
- [10] Daleiden J, Rangelov V, Irmer S, Romer F, Strassner M, Prott C, Tarraf A and Hillmer H 2002 Record tuning range of InP-based multiple air-gap MOEMS filter *Electron. Lett.* **38** 1270–1
- [11] Mateus C F R, Chrostowski L, Yang S, Pathak R and Chang-Hasnain C J 2002 Widely tuneable torsional optical filter *IEEE Photon. Technol. Lett.* **14** 819–21
- [12] Spisser A, Ledantec R, Seassal C, Leclercq J L, Benyattou T, Rondi D, Blondeau R, Guillot G and Viktorovitch P 1998 Highly selective and widely tuneable 1.55  $\mu\text{m}$  InP/air-gap micromachined Fabry–Perot filter for optical communications *IEEE Photon. Technol. Lett.* **10** 1259–61
- [13] Tay C J, Quan C, Gopal M, Shen L and Akkipeddi R 2008 Nanoindentation techniques in the measurement of mechanical properties of InP-based free-standing MEMS structures *J. Micromech. Microeng.* **18** 025015
- [14] Pruessner M W, Datta M, Amarnath K, Kanakaraju S and Ghodssi R 2005 Indium phosphide based MEMS end-coupled optical waveguide switches *17th Int. Indium Phosphide and Related Materials Conf. (Glasgow, Scotland, 2005)* pp 103–13
- [15] Pruessner M W, Siwak N, Amarnath K, Kanakaraju S, Chuang W-H and Ghodssi R 2006 End-coupled optical waveguide MEMS devices in the indium phosphide material system *J. Micromech. Microeng.* **16** 832–42
- [16] Streit D C, Oki A K, Gutierrez-Aitken A L, Grossman P C, Block T R, Chin P T, Lai R, Chen Y and Grundbacher R W 2000 Indium phosphide microelectronics—revolutionary technology for advanced telecommunications *Technology Review* pp 1–18
- [17] Leclercq J L, Garrigues M, Letartre X, Seassal C and Viktorovitch P 2000 InP-based MOEMS and related topics *J. Micromech. Microeng.* **10** 287–92
- [18] Seassal C, Leclercq J L and Viktorovitch P 1996 Fabrication of InP-based freestanding microstructures by selective surface micromachining *J. Micromech. Microeng.* **6** 261–5
- [19] Petersen K E 1982 Silicon as a mechanical material *Proc. IEEE* **70** 420–57
- [20] Fricke K, Peiner E, Chahoud M and Schlachetzki A 1999 Fracture properties of InP microcantilevers by hetero-micromachining *Sensors Actuators A: Phys.* **76** 395–402
- [21] Greek S, Gupta R and Hjort K 1999 Mechanical considerations in the design of a micromechanical tuneable InP-based WDM filter *J. Microelectromech. Syst.* **8** 328–34
- [22] Greek S, Hjort K, Schweitz J-A, Seassal C, Leclercq J L, Gendry M, Besland M P, Viktorovitch P, Figueat C, Souliere V and Monteil Y 1997 Strength of indium-phosphide-based microstructures *Proc. SPIE* **3008** 251–7
- [23] Pruessner M, King T T, Kelly D P, Grover R, Calhoun L C and Ghodssi R 2003 Mechanical property measurement of InP-based MEMS for optical communications *Sensors Actuators A: Phys.* **105** 190–200
- [24] Chitica N, Strassner M and Daleiden J 2000 Quantitative evaluation of growth-induced residual stress in InP epitaxial micromechanical structures *AIP* **77** 204–4
- [25] Judy J W 2001 Microelectromechanical systems (MEMS): fabrication, design and applications *Smart Mater. Struct.* **10** 1115–34
- [26] Hjort K 1996 Sacrificial etching of III–V compounds for micromechanical devices *J. Micromech. Microeng.* **6** 370–5
- [27] Chang-Hasnain C J 2000 Tuneable VCSEL *IEEE J. Sel. Top. Quantum Electron.* **6** 978–87
- [28] Hjort K 1997 Micromechanics in indium phosphide for opto electrical applications *Int. Semiconductor Conf. 1997. CAS'97 Proc. (Sinaia, Romania, 7–11 October 1997)* vol 2 pp 431–40
- [29] Hjort K, Soderkvist J and Schweitz J-A 1994 Gallium arsenide as a mechanical material *J. Micromech. Microeng.* **4** 1–13
- [30] Kelly D, Pruessner M W, Amarnath K, Datta M, Kanakaraju S, Calhoun L C and Ghodssi R 2004 Monolithic suspended optical waveguides for InP MEMS *IEEE Photon. Technol. Lett.* **16** 1298–300
- [31] Spahn O B, Sullivan C T, Bakke T, Allerman A, Reno J, Grossetete G, Lean J and Fuller C 2001 Promise and progress of GaAs MEMS and MOEMS *Digest GaAs Mantech*

- [32] Shah M A, Jisheng P, Shanmugan V and Akkipeddi R 2006 Fabrication of moisture-desensitized freestanding structures from InP for photonic-MEMS applications *J. Electrochem. Soc.* **153** G7
- [33] Pearton S J and Ren F 1994 Science of dry etching of III–V materials *J. Mater. Sci.: Mater. Electron.* **5** 1–12
- [34] Pearton S J, Ren F, Abernathy C R, Hobson W S, Fullowan T R, Esagvi R and Lothian J R 1992 Damage introduction in InP and InGaAs during Ar and H<sub>2</sub> plasma exposure *Appl. Phys. Lett.* **61** 586–8
- [35] Rommel S L, Jang J-H, Lu W, Cueva G, Zhou L, Adesida I, Pajer G, Whaley R, Lepore A, Schellanbarger Z and Abeles J H 2002 Effect of H<sub>2</sub> on the etch profile of InP/InGaAsP alloys in Cl<sub>2</sub>/Ar/H<sub>2</sub> inductively coupled plasma reactive ion etching chemistries for photonic device fabrication *J. Vac. Sci. Technol. B: Microelectron. Nanometer Struct.* **20** 1327
- [36] Carter A J, Thomas B, Morgan D V, Bhardwaj J K, McQuarrie A M and Stephens M A 1989 Dry etching of GaAs and InP for optoelectronic devices *IEE Proc. J. Optoelectron.* **136** 2–5
- [37] Keskinen J, Nappi J, Asonen H and Pessa M 1990 Methane/hydrogen metal organic reactive ion etching of GaInAsP compounds *Electron. Lett.* **26** 1369–71
- [38] Grover R, Hryniewicz J V, King O S and Van V 2001 Process development of methane–hydrogen–argon-based deep dry etching of InP for high aspect-ratio structures with vertical facet-quality sidewalls *J. Vac. Sci. Technol. B: Microelectron. Nanometer Struct.* **19** 1694
- [39] Grover R, Ibrahim T A, Ding T N, Leng Y, Kuo L-C, Kanakaraju S, Amarnath K, Calhoun L C and Ho P-T 2003 Laterally coupled InP-based single-mode microracetrack notch filter *IEEE Photon. Technol. Lett.* **15** 1082–4
- [40] Hahn Y, Hays D C, Cho H, Jung K B, Abernathy C R, Pearton S J and Shulb R J 1999 Effect of inert gas additive species on Cl<sub>2</sub> high density plasma etching of compound semiconductors Part II. InP, InSb, InGaP and InGaAs *Appl. Surf. Sci.* **147** 215–21
- [41] Adesida I, Nummala K, Andideh E, Hughes J, Caneau C, Bhat R and Holmstrom R 1990 Nanostructure fabrication in InP and related compounds *J. Vac. Sci. Technol. B: Microelectron. Nanometer Struct.* **8** 1357–60
- [42] Bouchoule S, Patriarche G, Guilet S, Gatilova L, Largeau L and Chabert P 2008 Sidewall passivation assisted by a silicon coverplate during Cl<sub>2</sub>–H<sub>2</sub> and HBr inductively coupled plasma etching of InP for photonic devices *J. Vac. Sci. Technol. B: Microelectron. Nanometer Struct.* **26** 666
- [43] Bouchoule S, Azouigui S, Guilet S, Patriarche G, Largeau L, Martinez A, Le Gratiat L, Lemaitre A and Lelarge F 2008 Anisotropic and smooth inductively coupled plasma etching of III–V laser waveguides using HBr–O<sub>2</sub> chemistry *J. Electrochem. Soc.* **155** H778
- [44] Docter B, Geluk E J, Karouta F and Smit M K 2006 Deep etching of DBR gratings in InP using Cl<sub>2</sub> based ICP processes *Proc. Symp. IEEE/LEOS Benelux Chapter (Eindhoven, the Netherlands)*
- [45] Deng L 2004 ICP etching of InP and related materials using photoresist as mask *Proc. SPIE* **5280** 838–43
- [46] Lee H W, Kim M, Min N-K, Efremov A, Lee C-W and Kwon K-H 2008 Etching characteristics and mechanism of InP in inductively coupled HBr/Ar plasma *Japan. J. Appl. Phys.* **47** 6917–22
- [47] Lim E L, Teng J H, Chong L F, Sutanto N, Chua S J and Yeoh S 2008 Inductively coupled plasma etching of InP with HBr/O<sub>2</sub> chemistry *J. Electrochem. Soc.* **155** D47
- [48] Lishan D, Lee J and Kim G 2001 InP processing using an HBr high density ICP plasma *GaAs MANTECH Conf. B* vol 9 p 4
- [49] Eun-Hyun P and Young-Se K 2000 Chemical etching of InGaAsP/InP using HBr–H<sub>3</sub>PO<sub>4</sub>–K<sub>2</sub>Cr<sub>2</sub>O<sub>7</sub> and its application to microlens array *Int. Conf. on Indium Phosphide and Related Materials, 2000*, pp 190–2
- [50] Sabin E, Elmadjian R and Grumman N 2003 The by-products and etching species from plasma etching of InP using HBr *204th Meeting of the Electrochemical Society, 2003 (Orlando, FL, 12–16 October 2003)* p Abs. 759
- [51] Sultana N, Zhou W, LaFave T P and MacFarlane D L 2009 HBr based inductively coupled plasma etching of high aspect ratio nanoscale trenches in InP: considerations for photonic applications *J. Vac. Sci. Technol. B: Microelectron. Nanometer Struct.* **27** 2351
- [52] Vicknesh S and Ramam A 2004 Etching characteristics of HBr-based chemistry on InP using the ICP technique *J. Electrochem. Soc.* **151** 772–80
- [53] Matsutani A, Htsuki H O, Uta S M, Oyama F K and Ga K I 2001 Mass effect of etching gases in vertical and smooth dry etching of InP *Japan. J. Appl. Phys.* **40** 1528–9
- [54] Pruessner M W, King T, Kelly D, Grover R, Calhoun L C and Ghodssi R 2003 Mechanical property measurement of InP-based MEMS for optical communications *Sensors Actuators A* **105** 190–200
- [55] Gatilova L, Bouchoule S, Guilet S and Chabert P 2009 Investigation of InP etching mechanisms in a Cl<sub>2</sub>/H<sub>2</sub> inductively coupled plasma by optical emission spectroscopy *J. Vac. Sci. Technol. A: Vac. Surf. Films* **27** 262
- [56] Guilet S, Lee K H, Patriarche G, Talneau A and Bouchoule S 2008 Role of nitrogen in chlorine based plasma for InP dry etching *Symp. on Emerging Technologies for Micro-Nanofabrication (Toulouse, France, 2008)*
- [57] Karouta F, Docter B, Geluk E J, Sander-Jochem M J H, van der Tol J J G M and Smit M K 2005 Role of temperature and gas-chemistry in micro-masking of InP by ICP etching *Proc. 18th IEEE LEOS Annual Meeting 2005* pp 987–8
- [58] Shul R, Baca A, Rieger D, Hou H, Pearton S and Ren F 1996 ECR etching of GaP, GaAs, InP, and InGaAs in Cl<sub>2</sub>/Ar, Cl<sub>2</sub>/N<sub>2</sub>, BCl<sub>3</sub>/Ar, and BCl<sub>3</sub>/N<sub>2</sub> *MRS Proceedings* vol 421 p 245
- [59] Yoshikawa T, Kohmoto S, Ozaki M, Hamao N, Sugimoto Y, Sugimoto M and Asakawa K 1992 Smooth and vertical InP reactive ion beam etching with Cl<sub>2</sub> ECR plasma *Japan. J. Appl. Phys.* **31** L655
- [60] Tran A T T D, Lo Y H, Zhu Z H, Haronian D and Mozdy E 1996 Surface micromachined Fabry–Perot tunable filter *IEEE Photon. Technol. Lett.* **8** 393–5
- [61] Larson M C, Pezeshki B and Harris J S Jr 1995 Vertical coupled-cavity microinterferometer on GaAs with deformable-membrane top mirror *IEEE Photon. Technol. Lett.* **7** 382–4
- [62] LeDantec R, Benyattou T, Guillot G, Spisser A, Seassal C, Leclercq J L, Viktorovitch P, Rondi D and Blondeau R 1999 Tunable microcavity based on InP-air Bragg mirrors *IEEE J. Sel. Top. Quantum Electron.* **5** 111–4
- [63] Bondavalli P, LeDantec R and Benyattou T 2001 Influence of the involuntary underetching on the mechanical properties of tunable Fabry–Pérot filters for optical communications *J. Microelectromech. Syst.* **10** 298–301
- [64] Strassner M, Daleiden J, Chitica N, Keiper D, Stålnacke B, Greek S and Hjort K 2000 III–V semiconductor material for tunable Fabry–Perot filters for coarse and dense WDM systems *Sensors Actuators A: Phys.* **85** 249–55
- [65] Irmer S, Daleiden J, Rangelov V, Prott C, Römer F, Strassner M, Tarraf A and Hillmer H 2003 Ultralow biased widely continuously tunable Fabry–Pérot filter *IEEE Photon. Technol. Lett.* **15** 434–6
- [66] Datta M, Pruessner M W, Kelly D and Ghodssi R 2004 Design of MEMS-tunable novel monolithic optical filters in InP with horizontal Bragg mirrors *Solid State Electron.* **48** 1959–63

- [67] Kelly D P, Pruessner M W, Amarnath K, Datta M, Kanakaraju S, Calhoun L C and Ghodssi R 2004 Monolithic suspended optical waveguides for InP MEMS *IEEE Photon. Technol. Lett.* **16** 1298–300
- [68] Datta M, Pruessner M W, Amarnath K, McGee J, Kanakaraju S and Ghodssi R 2005 Wavelength-selective integrated optical MEMS filter in InP *18th Int. Conf. on Micro Electro Mechanical Systems (Miami Beach, FL, 2005)* pp 88–91
- [69] McGee J, Siwak N, Morgan B and Ghodssi R 2005 In-plane indium phosphide tunable optical filter using ridge waveguides *2005 International Semiconductor Device Research Symposium (Bethesda, MD, December 2005)* pp 56–7
- [70] Zhou G and Dowd P 2003 Tilted folded-beam suspension for extending the stable travel range of comb-drive actuators *J. Micromech. Microeng.* **13** 178–83
- [71] Lackner M, Schwarzott M, Winter F, Kögel B, Jatta S, Halbritter H and Meissner P 2006 CO and CO<sub>2</sub> spectroscopy using a 60 nm broadband tunable MEMS-VCSEL at  $\sim 1.55 \mu\text{m}$  *Opt. Lett.* **31** 3170–2
- [72] Kogel B, Halbritter H, Jatta S, Maute M, Bohm G, Amann M-C, Lackner M, Schwarzott M, Winter F and Meissner P 2007 Simultaneous spectroscopy of NH<sub>3</sub> and CO Using a  $>50$  nm continuously tunable MEMS-VCSEL *IEEE Sensors J.* **7** 1483–9
- [73] Grundl T *et al* 2013 Continuously tunable, polarization stable SWG MEMS VCSELs at  $1.55 \mu\text{m}$  *IEEE Photon. Technol. Lett.* **25** 841–3
- [74] Gruendl T, Zogal K, Debernardi P, Gierl C, Grasse C, Geiger K, Meyer R, Boehm G, Amann M-C, Meissner P and Kueppers F 2013 50 nm continuously tunable MEMS VCSEL devices with surface micromachining operating at  $1.95 \mu\text{m}$  emission wavelength *Semicond. Sci. Technol.* **28** 012001
- [75] Gierl C, Grundl T, Zogal K, Davani H A, Grasse C, Bohm G, Kueppers F, Meissner P and Amann M C 2011 Surface micromachined MEMS-tunable VCSELs with wide and fast wavelength tuning *Electron. Lett.* **47** 1243–4
- [76] Paul S, Gierl C, Grundl T, Zogal K, Meissner P, Amann M-C and Kueppers F 2013 Far-field emission characteristics and linewidth measurements of surface micro-machined MEMS tunable VCSELs *Proc. SPIE* **8639** 86390H
- [77] Tay C J, Quan C, Liu H, Gopal M and Akkipeddi R 2010 Stress gradient of a micro-optoelectromechanical systems Fabry–Perot cavity based on InP *J. Micro/Nanolith. MEMS MOEMS* **9** 023010-023010
- [78] de Dooda M J A, Polman A, Zijlstra T and van der Drift E W J M 2002 Amorphous silicon waveguides for microphotronics *J. Appl. Phys.* **92** 649–53
- [79] Deri R J and Kapon E 1991 Low-loss III–V semiconductor optical waveguides *IEEE J. Quantum Electron.* **27** 626–40
- [80] Dupont S, Beaurain A, Miska P, Zegaoui M, Vilcot J, Li H W, Constant M, Decoster D and Chazelas J 2004 Low-loss InGaAsP/InP submicron optical waveguides fabricated by ICP etching *Electron. Lett.* **40** 865–6
- [81] Kubby J A 2002 Advances in MEMS integration with planar waveguide devices *Symp. on Integrated Optoelectronic Devices (Int. Soc. for Optics and Photonics)* pp 1–12
- [82] Makihara M 2000 Microelectromechanical intersecting waveguide optical switch based on thermo-capillarity *2000 IEEE/LEOS Conf. on Optical MEMS (Lugano, Switzerland, 2000)* pp 33–4
- [83] Noh J W, Anderson R, Kim S, Cardenas J and Nordin G P 2008 In-plane photonic transduction of silicon-on-insulator microcantilevers *Opt. Express* **16** 12114–23
- [84] Ollier E 2002 Optical MEMS devices based on moving waveguides *IEEE J. Sel. Top. Quantum Electron.* **8** 155–62
- [85] Stievater T H, Rabinovich W S, Park D, Khurgin J B, Kanakaraju S and Richardson C J K 2008 Low-loss suspended quantum well waveguides *Opt. Express* **16** 2621–7
- [86] Ng W H, Podoliak N, Stewart W, Horak P, Liu H and Kenyon A J 2014 Design and fabrication of InP free-standing optical waveguides for MEMS *2014 International Conference on Optical MEMS and Nanophotonics (OMN) (Glasgow, UK, 17–21 August 2014)* pp 181–2
- [87] Ollier E, Labeye P and Revol F 1995 Micro-opto mechanical switch integrated on silicon *Electron. Lett.* **31** 2003–5
- [88] Chen R T, Nguyen H and Wu M C 1999 A high-speed low-voltage stress-induced micromachined  $2 \times 2$  optical switch *IEEE Photon. Technol. Lett.* **11** 1396–8
- [89] Chinni V R, Huang T C, Wai P K A, Menyuk C R and Simonis G J 1995 Performance of field-induced directional coupler switches *IEEE J. Quantum Electron.* **31** 2068–74
- [90] Mizuno T, Takahashi H, Kitoh T, Oguma M, Kominato T and Shibata T 2005 Mach–Zehnder interferometer switch with a high extinction ratio over a wide wavelength range *Opt. Lett.* **30** 251–3
- [91] Nielson G N, Seneviratne D, Lopez-Royo F, Rakich P T, Giacometti F, Tuller H L and Barbastathis G 2004 MEMS based wavelength selective optical switching for integrated photonic circuits *Conference on Lasers and Electro-Optics (CLEO) (San Francisco, CA, 2004)*
- [92] Povinelli M L *et al* 2003 Design of a nanoelectromechanical high-index-contrast guided wave optical switch for single-mode operation at  $1.55 \mu\text{m}$  *IEEE Photon. Technol. Lett.* **15** 1207–9
- [93] Pruessner M W, Amarnath K, Datta M, Kelly D, Kanakaraju S, Ho P-T and Ghodssi R 2005 InP-based optical waveguide MEMS switches with evanescent coupling mechanism *J. Microelectromech. Syst. (JMEMS)* **14** 1070–81
- [94] Pruessner M W, Amarnath K, Datta M, Kelly D P, Kanakaraju S, Ho P-T and Ghodssi R 2004 Optical and mechanical characterization of an evanescent coupler optical switch *Solid-State Sensor, Actuator and Microsystems Workshop (Hilton Head, SC, 2004)* pp 238–41
- [95] Saini S S, Johnson F G, Stone D R, Zhou W, Shen H and Dagenais M 2001 A  $2 \times 2$  crosspoint switch fabricated on the passive active resonant coupler (PARC) platform *IEEE Photon. Technol. Lett.* **13** 203–5
- [96] Shubin I and Wa P L K 2001 Electrostatically actuated  $1 \times 2$  micromechanical optic switch *Electron. Lett.* **37** 451–2
- [97] Bakke T, Tigges C P, Lean J J, Sullivan C T and Spahn O B 2002 Planar microoptomechanical waveguide switches *IEEE J. Sel. Top. Quantum Electron.* **8** 64–72
- [98] Bakke T, Tigges C P and Sullivan C T 2002  $1 \times 2$  MOEMS switch based on silicon-on-insulator and polymeric waveguides *Electron. Lett.* **38** 177–8
- [99] Podoliak N, Ng W, Liu H, Kenyon A, Stewart W and Horak P 2014 MEMS actuation for a continuously tunable optical buffer *2014 International Conference on Optical MEMS and Nanophotonics (OMN) (Glasgow, UK, 17–21 August)* pp 103–4
- [100] Zinoviev K, Dominguez C, Plaza J A, Busto V J C and Lechuga L M 2006 A novel optical waveguide microcantilever sensor for the detection of nanomechanical forces *J. Light. Technol.* **24** 2132–8
- [101] Ilic B, Craighead H G, Krylov S, Senaratne W, Ober C and Neuzil P 2004 Attogram detection using nanoelectromechanical oscillators *J. Appl. Phys.* **95** 3694–703
- [102] Ilic B, Czaplewski D, Zalalutdinov M, Craighead H G, Neuzil P, Campagnolo C and Batt C 2001 Single cell detection with micromechanical oscillators *J. Vac. Sci. Technol. B: Microelectron. Nanometer Struct.* **19** 2825–8

- [103] Ilic B, Yang Y and Craighead H G 2004 Virus detection using nanoelectromechanical devices *Appl. Phys. Lett.* **85** 2604
- [104] Ilic B R, Krylov S, Kondratovich M and Craighead H G 2007 Optically actuated nanoelectromechanical oscillators *IEEE J. Sel. Top. Quantum Electron.* **13** 392–9
- [105] Lavrik N V and Datskos P G 2003 Femtogram mass detection using photothermally actuated nanomechanical resonators *Appl. Phys. Lett.* **82** 2697
- [106] Lavrik N V, Sepaniak M J and Datskos P G 2004 Cantilever transducers as a platform for chemical and biological sensors *Rev. Sci. Instrum.* **75** 2229
- [107] Koev S T, Fernandes R, Bentley W E and Ghodssi R 2009 A cantilever sensor with an integrated optical readout for detection of enzymatically produced homocysteine *IEEE Trans. Biomed. Circuits Syst.* **3** 415–23
- [108] Nordström M, Zauner D A, Calleja M, Hubner J and Boisen A 2007 Cantilever-based sensor with integrated optical readout using single mode waveguides *11th Int. Conf. on Miniaturized Systems for Chemistry and Life Sciences (Paris, France, 7–11 October 2007)* pp 497–9
- [109] Xu T, Bachman M, Zeng F-G and Li G-P 2003 Polymeric micro-cantilever acoustic sensor array *TRANSDUCERS '03. 12th Int. Conf. on Solid-State Sensors, Actuators and Microsystems (Boston, MA, 8–12 June 2003)* vol 2, pp 1116–9
- [110] Jiang F, Keating A, Martyniuk M, Pratap R, Faraone L and Dell J M 2013 Process control of cantilever deflection for sensor application based on optical waveguides *J. Microelectromech. Syst.* **22** 569–79
- [111] Siwak N, Hines D, Kanakaraju S, Goldsman N and Ghodssi R 2009 Indium phosphide MEMS cantilever resonator sensors utilizing a pentacene absorption layer *J. Microelectromech. Syst.* **18** 103–10
- [112] Siwak N P, Fan X Z, Kanakaraju S, Richardson C J K and Ghodssi R 2014 Indium phosphide-based monolithically integrated PIN waveguide photodiode readout for resonant cantilever sensors *Appl. Phys. Lett.* **105** 143102
- [113] Siwak N, Fan X Z and Ghodssi R 2011 Fabrication processes and technologies for monolithic InP microsystems *1st EOS Topical Meeting on Micro- and Nano-Optoelectronic Systems (Bremen, Germany, 7–9 December 2011)*
- [114] Apiratikul P, He L and Richardson C 2013 2  $\mu\text{m}$  laterally coupled distributed-feedback GaSb-based metamorphic laser grown on a GaAs substrate *Appl. Phys. Lett.* **102** 231101
- [115] Amarnath K, Grover R, Kanakaraju S and Ho P-T 2005 Electrically pumped InGaAsP–InP microring optical amplifiers and lasers with surface passivation *IEEE Photon. Technol. Lett.* **17** 2280–2
- [116] Demir H V, Zheng J-F, Sabnis V A, Fidaner O, Hanberg J, Harris J S and Miller D A 2005 Self-aligning planarization and passivation for integration applications in III–V semiconductor devices *IEEE Trans. Semicond. Manuf.* **18** 182–9
- [117] Liu W, Lubyshev D, Fastenau J, Wu Y, Bulsara M, Fitzgerald E, Urteaga M, Ha W, Bergman J and Brar B 2009 Monolithic integration of InP-based transistors on Si substrates using MBE *J. Cryst. Growth* **311** 1979–83
- [118] Porkolab G, Chen Y, Tabatabaei S A, Agarwala S, Johnson F, King O, Dagenais M, Frizzell R E, Beard W Jr and Stone D 1997 Air-bridges, air-ramps, planarization, and encapsulation using pyrolytic photoresist in the fabrication of 3D microstructures *J. Vac. Sci. Technol. B* **15** 1961–5
- [119] Porkolab G, Hsu S H, Hryniewicz J V, Lin W, Chen Y, Agarwala S, Johnson F, King O, Dagenais M and Stone D 1996 Etch-mask of pyrolytic-photoresist thin-film for self-aligned fabrication of smooth and deep faceted 3D microstructures *J. Vac. Sci. Technol. B* **14** 3650–3
- [120] Siwak N, Fan X, Kanakaraju S, Richardson C and Ghodssi R 2014 Indium phosphide-based monolithically integrated PIN waveguide photodiode readout for resonant cantilever sensors *Appl. Phys. Lett.* **105** 143102
- [121] Kusserow T, Wulf M, Zamora R, Kanwar K and Hillmer H 2013 Processing of photonic crystals in InP membranes by focused ion beam milling and plasma etching *Microelectron. Eng.* **102** 25–8
- [122] Marsh J H 1993 Quantum well intermixing *Semicond. Sci. Technol.* **8** 1136–55
- [123] Liang D, Bowers J E, Oakley D C, Napoleone A, Chapman D C, Chen C-L, Juodawlkis P W and Raday O 2009 High-quality 150 mm InP-to-silicon epitaxial transfer for silicon photonic integrated circuits *Electrochem. Solid-State Lett.* **12** H101–4
- [124] Liang D, Fang A, Chen H-W, Sysak M, Koch B, Lively E, Raday O, Kuo Y-H, Jones R and Bowers J 2009 Hybrid silicon evanescent approach to optical interconnects *Appl. Phys. A: Mater. Sci. Process.* **95** 1045–57
- [125] Heck M J R, Hui-Wen C, Fang A W, Koch B R, Di L, Hyundai P, Sysak M N and Bowers J E 2011 Hybrid silicon photonics for optical interconnects *IEEE J. Sel. Top. Quantum Electron.* **17** 333–46
- [126] Creazzo T, Marchena E, Krasulick S B, Yu P K, Van Orden D, Spann J Y, Blivin C C, He L, Cai H and Dallesasse J M 2013 Integrated tunable CMOS laser *Opt. Express* **21** 28048–53
- [127] Anantha P and Tan C S 2014 Homogeneous chip to wafer bonding of InP–Al<sub>2</sub>O<sub>3</sub>–Si using UV/O<sub>3</sub> activation *ECS J. Solid State Sci. Technol.* **3** P43–7